Structure
Article

Crystal Structures of the N-Terminal Domains of Cardiac and Skeletal Muscle Ryanodine Receptors: Insights into Disease Mutations

Paolo Antonio Lobo[1] and Filip Van Petegem[1,*]
[1]University of British Columbia, Department of Biochemistry and Molecular Biology, Vancouver, BC V6T 1Z3 Canada
*Correspondence: filip.vanpetegem@gmail.com
DOI 10.1016/j.str.2009.08.016

SUMMARY

Ryanodine receptors (RyRs) are channels governing the release of Ca^{2+} from the sarcoplasmic or endoplasmic reticulum. They are required for the contraction of both skeletal (RyR1) and cardiac (RyR2) muscles. Mutations in both RyR1 and RyR2 have been associated with severe genetic disorders, but high-resolution data describing the disease variants in detail have been lacking. Here we present the crystal structures of the N-terminal domains of both RyR2 (1–217) and RyR1 (9–205) at 2.55 Å and 2.9 Å, respectively. The domains map in a hot spot region for disease mutations. Both structures consist of a core beta trefoil domain flanked by an alpha helix. Crystal structures of two RyR2 disease mutants, A77V (2.2 Å) and V186M (1.7 Å), show that the mutations cause distinct local changes in the surface of the protein. A RyR2 deletion mutant causes significant changes in the thermal stability. The disease positions highlight two putative binding interfaces required for normal RyR function.

INTRODUCTION

Excitation-contraction (E-C) coupling in skeletal muscle and cardiac myocytes requires the release of Ca^{2+} into the cytoplasm. Ryanodine receptors (RyRs) are large (~2.2 MDa) membrane proteins that mediate the release of Ca^{2+} from the sarcoplasmic or endoplasmic reticulum. Three different isoforms (RyR1–3) have been identified in mammalian organisms. RyR1 predominates in skeletal muscle, whereas RyR2 regulates Ca^{2+} release in cardiac myocytes (Giannini et al., 1995). Each intact RyR is a homotetramer built up by polypeptides of >5000 amino acids each. In addition, many auxiliary proteins associate with the channels and regulate their activity (Bers, 2004; Zalk et al., 2007).

In skeletal muscle, mutations in RyR1 are known to lead to malignant hyperthermia (MH) and central core disease (CCD) (Robinson et al., 2006), whereas the cardiac RyR2 mutations have been associated with two forms of cardiac arrhythmia—catecholaminergic polymorphic ventricular tachycardia (CPVT) and arrhythmogenic right ventricular dysplasia type 2 (ARVD2) (George et al., 2007; Thomas et al., 2007). The mutations were originally found to be clustered in three distinct regions, giving rise to mutational "hot spots" in the N-terminal region (~1–600), a central domain (~2100–2500), and the C-terminal channel region (~3800–5000). Sequence alignment of RyR1 and RyR2 shows that the hot spots are matching (Yano, 2008), although mutations in RYR1 are increasingly found outside the original hot spots (Robinson et al., 2006). Some mutations even occur in both isoforms, suggesting that RyR1 and RyR2 share similar mechanisms.

High-quality electron microscopy (EM) experiments have shed light on the 3D structure of RyRs, especially for RyR1 (Ludtke et al., 2005; Samso et al., 2005). The bulk of the RyR structure is located in the cytoplasm, with only 10% forming the transmembrane and channel pore regions. EM images of RyR2 and RyR3 show a similar overall structure, although some differences exist in the corners of the cytoplasmic portion (Liu et al., 2001; Sharma et al., 1998; Wang et al., 2007). Many distinct blobs are present in the EM structures, suggesting that the RyR protein is built up by individual domains. However, atomic resolution information has only recently become available (Amador et al., 2009; Maximciuc et al., 2006; Wright et al., 2008). The limited availability of high-resolution information has hampered a detailed understanding of RyR function in physiological and diseased states.

Here we describe crystal structures for the N-terminal domains of RyR1 and RyR2. This domain is located in the N-terminal mutation hot spot. We also solved the crystal structures of two RyR2 disease mutants, putting us in the unique position to look at the effect of disease mutations on a eukaryotic ion channel at high resolution. The mutations highlight distinct interaction interfaces on the surface of the RyR2 N-terminal domain. Two flexible cysteine pairs seem to be poised to undergo oxidation or receive modifications.

RESULTS

Overall Structure of the RyR2 N-Terminal Domain

We solved the crystal structure of the N-terminal domain (NTD) of mouse RyR2 (residues 1–217) at 2.55 Å resolution (Figures 1A and 1B and Table 1). The crystal structure contains two chains in the asymmetric unit. All structural analysis given below is performed with the slightly more complete chain B. Central in the NTD structure is a β-trefoil core, consisting of 12 β strands, which is held together through extensive hydrophobic packing. The N-terminal 11 residues form a flexible stretch with no

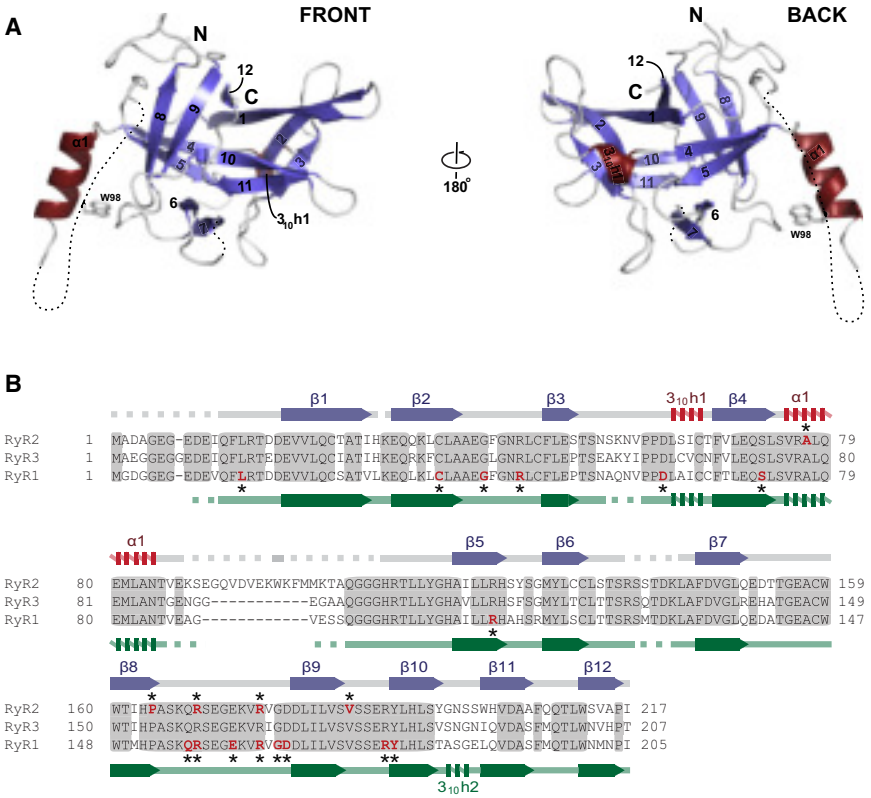

Figure 1. Overall Structure of the RyR NTD

(A) Overall fold of the RyR2 NTD, showing the α helix (α1) and 3_{10} helix (3_{10}h1) in red, β strands in blue, and loops in white. Two views are shown (labeled "front" and "back"), rotated 180° around a vertical axis. All β strands are labeled for reference. Loops present in the construct but not modeled are shown as dotted lines. W98 in the α1-β5 loop is shown in stick representation. The positions of the amino- and carboxytermini are indicated.

(B) Sequence alignment of the NTD of mouse RyR2, rabbit RyR1, and human RyR3. Conserved residues are highlighted in gray. Secondary structure elements are shown on top (RyR2) and at the bottom (RyR1). Sequence stretches present in the constructs but not modeled in the electron density are shown as dotted lines. Positions found in disease mutations are marked with an asterisk and highlighted in red.

(C) Superposition of the backbone trace of RyR1 (green) and RyR2 NTD (blue). Loops with conformational changes are highlighted. The view is the same as the front view of Figure 1A.

interpretable electron density. The core is flanked by a 10-residue α helix that is inserted between strands β4 and β5. In addition, a small three-residue 3_{10} helix is present in the loop connecting β3 and β4.

The α helix packs against the β-trefoil core, burying a total of ~640 Å^2 of solvent accessible surface area. The major interaction is formed by L78 on the helix and W159 on the core, two residues that are conserved between the three RyR isoforms. Although the helix is pointing away from the trefoil core, the extensive packing suggests that its relative position is fixed.

A long loop connects the α helix back to β5. Although electron density is present for this loop, it is not of sufficient quality to build a reliable model for this region, suggesting that the loop has a high degree of flexibility (see Figures S1B and S1C available online). The exception is a single tryptophan residue (W98), which packs in a hydrophobic pocket, lined by the conserved L78 and W159 residues, next to the α helix (Figure 1A; Figure S1B) (see Experimental Procedures). This tryptophan residue, and the loop to which it belongs, are unique to RyR2.

RyR1 Versus RyR2

Are the structural features in the RyR2 NTD conserved among different RyR isoforms? To answer this question, we solved the structure of the rabbit RyR1 NTD (residues 9–205) to 2.9 Å resolution. The RyR1 NTD structure contains nine molecules in the asymmetric unit. Because all molecules intrinsically experience different crystal contacts, this allows us to deduce which parts of the protein are rigid (Figure S2A). Within the nine chains, all β strands and the α helix superpose well, but some conformational differences are present in the loops connecting β1-β2 and β10-β11, suggesting that these loops have some degree of flexibility.

Both the RyR1 and RyR2 NTD display the same overall fold and can be superposed with a RMSD of 0.9 Å for 164 Cα atoms (using RyR1 chain A) (Figure 1C). Even though crystal contacts are different, the relative orientation of the α helix to the β-trefoil core is the same for both RyR2 and the nine chains of the RyR1 asymmetric unit. This finding confirms the rigidity of the helix in the structure.

Despite the overall similarity, a number of differences exist in the loops connecting the various β strands. The major difference is a 12-residue insertion in the large loop connecting helix α1 with β5 (Figure 1B). The W98 residue, which binds next to the α helix in RyR2, is therefore not present in the RyR1 sequence and, correspondingly, no electron density was observed in any of the 9 RyR1 chains. An additional short 3_{10} helix is present in the RyR1 loop connecting β10-β11. Both loops connecting

Table 1. Data Collection and Refinement Statistics

	RyR2 V186M	RyR2 A77V	RyR2 WT	RyR1 WT
Wavelength (Å)	0.97949	0.97949	0.97934	0.97949
Resolution (Å)	50–1.70 (1.73–1.70)	50–2.2 (2.28–2.20)	50–2.55 (2.64–2.55)	50–2.9 (3.0–2.9)
Space group	$I4_1$	$I4_1$	C2	$P2_1$
Cell parameters (Å,°)	a = b = 112.5	a = b = 112.2	a = 155.0 b = 39.0	a = 70.73 b = 155.71
	c = 36.8	c = 36.8	c = 107.6	c = 81.61
	α = β = γ = 90	α = β = γ = 90	α = γ = 90 β = 131.8	α = γ = 90 β = 110.6
No. of unique reflections	25132 (1273)	10981 (687)	15222 (945)	34226 (2509)
R_{sym} (%)[a]	10.1 (57.7)	7.6 (38.8)	9.6 (38.1)	14.6 (40.8)
I/σ(I)	20.6 (2.4)	13.9 (2.5)	19.2 (2.2)	12.37 (2.9)
Completeness (%)	99.7 (100)	93.3 (59.8)	93.6 (58.5)	92.8 (68.2)
Mosaicity (°)	0.52	0.78	1.0	0.45
R_{cryst}/R_{free} (%)	20.1/24.4	22.3/27.5	22.1/28.8	27.4/32.0
No. of protein residues	175	174	349	1394
No. of water molecules	99	31	34	0
Bond lengths RMSD (Å)	0.030	0.014	0.009	0.005
Bond angles RMSD (°)	2.44	1.57	1.23	0.784
Mean overall B value ($Å^2$)	23.1	27.7	30.3	68.0
% Residues in core/allowed regions of Ramachandran plot	94.1/5.9	91.5/8.5	92.9/7.8	92.2/7.8

Values in parentheses refer to the highest resolution shell, where applicable.
[a] $R_{sym} = \Sigma_h \Sigma_i | I(h,i) - < I(h) > | / \Sigma_h \Sigma_i I(h,i)$, where I(h,i) is the intensity of the *i*th measurement of reflection *h* and < I(h) > is the average value over multiple measurements.

β1-β2 and β10-β11 display different conformations, compared with RyR2.

Thermal Stability

In humans, particular RyR2 mutations have been shown to cause CPVT and ARVD2. At least five of these mutations are located in the RyR2 NTD. One obvious and trivial explanation for a disease phenotype is a general destabilization of the domain. We therefore measured thermal melting curves for both wild-type and mutant NTDs using thermofluor experiments (Nettleship et al., 2008). Wild-type RyR2 NTD has a melting temperature of ~57°C (Figures 2A and 2B and Table 2). None of the five point mutations significantly alters the melting temperature. However, there is a big discrepancy between the three RyR isoforms, because the RyR1 NTD has a melting temperature of 46°C, significantly lower than those for RyR2 and RyR3 NTDs. Although RyR1 and RyR2 share the same overall fold, the stability seems to be drastically different. This correlates with the ability of the proteins to crystallize, because RyR2 crystals are easier to obtain and have a better diffraction quality. However, the reasons for the difference in thermal stability are not clear.

Structure of RyR2 Disease Mutants A77V and V186M

Because none of the disease-causing point mutations of RyR2 seems to affect the domain stability, we wondered whether they would alter the global or local structure of the domain. To this extent, we solved the structures of two RyR2 NTD disease mutants, A77V and V186M, to 2.2 Å and 1.7 Å, respectively, allowing us to analyze the effects of the mutations in detail.

Superposition of both mutants with the wild-type shows that the overall structure is conserved, with RMSD values of ~0.7 Å for 179 (A77V) and 188 (V186M) Cα atoms. The main exception is the β8-β9 loop (Figure S2B). Because mutants and wild-type

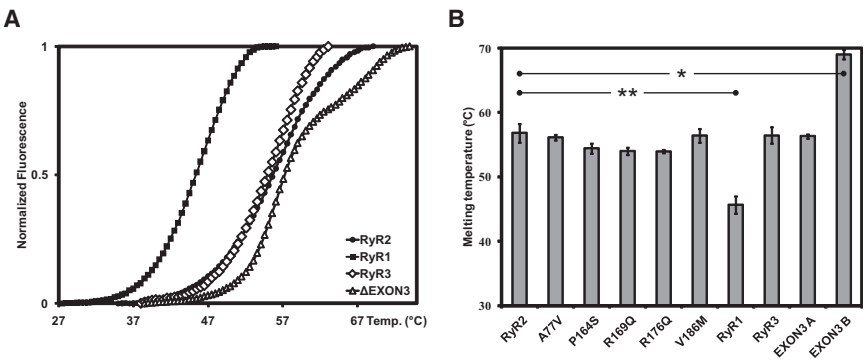

Figure 2. Thermal Stability of RyR NTDs
(A) Thermofluor experiments showing thermal melts for the NTD of RyR1 (filled squares), RyR2 (filled circles), RyR3 (open squares), and RyR2 Δexon 3 (open triangles).
(B) Measured melting temperatures for various wild-type and mutant NTDs. *$p < 10^{-5}$; **$p < 10^{-6}$ (one-tail student t test). Error bars show the standard deviations. The values are shown in Table 2. All point mutants are for the RyR2 NTD. Two transitions with separate melting temperatures were present for RyR2 Δexon3.

Table 2. Melting Temperatures for RyR NTDs

Name	Mean (°C)	Standard Deviation (°C)	n
RYR2	56.82	1.47	4
RYR1	45.68	1.06	6
RYR3	56.46	1.28	4
A77V	56.15	0.41	4
P164S	54.42	0.80	4
R169Q	54.00	0.57	4
R176Q	53.98	0.26	4
V186M	56.42	1.06	4
ΔEXON3 A	56.33	0.33	4
ΔEXON3 B	69.03	0.75	4

Measured melting temperatures for the NTD of the three RyR isoforms and various RyR2 mutants. The RyR2 Δexon3 mutant displays 2 distinct transitions (A and B).

crystallized in different space groups, this difference is likely due to variations in crystal contacts. Indeed, the loop is involved in crystal contacts for both A77V and V186M.

However, both positions are solvent exposed and cause distinct local changes to the protein surface. The A77V mutation introduces two extra methyl groups at the N-terminal end of helix α1 (Figure 3A), exposing ~33 Å^2 to the solvent. The mutation is mostly surrounded by hydrophilic residues, including an ionic pair between R76 and E80. Neighboring hydrophobic residues include M81 and L73 that are in Van der Waals contact with A77. Only small rearrangements take place in the neighboring residues to accommodate the extra volume. The main effect of the A77V mutation is therefore a distinct change in the surface at the bottom of the helix (Figure 3C).

The V186 residue is present at the bottom of a deep pocket that sits next to the N-terminal end of the α helix (Figure 3B). It is surrounded by both hydrophilic and hydrophobic residues, including L78 and W159, that stabilize the α helix orientation. The V186 side chain is pointing inward but is partially exposed to solvent. Upon mutation to methionine, there is insufficient space for this longer side chain to point inward. The M186 therefore curls back toward the surface and fills up a part of the deep pocket (Figure 3D).

Because neither mutant affects the overall structure or stability, the only possibility remaining is that they are located at an interface for transient or permanent domain-domain or protein-protein interactions. The N-terminal part of the α helix and the neighboring deep pocket therefore highlight sites required for normal RyR function.

The β8-β9 Loop Contains Many Disease Mutations

Three other RyR2 disease mutations have been found in the RyR2 NTD: P164S, R169Q, and R176Q. Although we have been able to crystallize all three mutants, the diffraction limit was too low to build reliable models. However, their ability to crystallize in the same condition with similar crystal morphology strongly suggests that the overall structures are not significantly altered.

Interestingly, all three mutations map to a 16-residue long loop connecting β8 and β9 (Figure 4A). P164 marks the beginning of the loop, whereas R169 and R176 are part of a small network of ionic pairs and hydrogen bonds, which include E173 and D179. The corresponding mutations are therefore expected to break the ionic interactions. The β8-β9 loop has an overall positive charge in both RyR1 and RyR2 (Figure 4B; Figure S3). Interestingly, a number of RyR1 disease mutations map to the same loop. Mutations in R156 and R163 correspond to RyR2 residues R169 and R176. The two acidic residues involved in the ionic pairs have also been reported to cause MH or CCD (human mutations E160G, D166N and D166G) (Rueffert et al., 2002; Shepherd et al., 2004). The β8-β9 loop therefore seems to play a significant role in RyR function and is likely part of a protein-protein or domain-domain interface.

In addition to mutations in the β8-β9 loop, other RyR1 disease mutations are more scattered across the surface, compared with RyR2 (Figures 4C and 4D). One of these, L14R, replaces a leucine residue, part of a hydrophobic core, by a longer arginine side chain (Robinson et al., 2006). As a result of steric hindrance, it is expected that such a mutation would destabilize the domain or cause major rearrangements in the neighboring environment. However, most of the RyR1 disease positions have some degree of surface exposure and may, therefore, be located at interaction sites.

Delta Exon3 Mutant

An unusual cause of CPVT is the deletion of an entire exon from the RyR2 gene (Bhuiyan et al., 2007; Marjamaa et al., 2009). The Δexon3 mutant abolishes RyR2 residues 57–91, thus removing a drastic portion of the RyR2 NTD structure (Figure 4C). The structural elements that are removed include the 3_{10} helix, β4, the α helix, and seven residues of the following flexible loop. β4 in particular seems to be a crucial element for maintaining the overall fold through main chain hydrogen bonding with the neighboring strands β1 and β5. Overall, residues in exon3 are responsible for 36 hydrogen bonds in the structure. A likely cause for the disease phenotype is therefore complete destabilization of the domain, causing misfolding. To test this idea, we expressed the domain in *Escherichia coli* like wild-type protein. Unexpectedly, this Δexon3 RyR2 NTD is soluble and could readily be purified. There are no indications for aggregation, because the protein runs as a single monomeric species on a gel filtration column (Figure S4). We next measured the thermal stability and found the protein to have two distinct transitions in the melting curve, one with a melting temperature similar to the wild-type RyR2 and one with a higher temperature of 69°C (Figures 2A and 2B; Table 2). This finding suggests the presence of two distinct subdomains within the Δexon3 mutant, including one with improved stability. Because the structural rearrangements in this mutant are likely to be very large, it is impossible to deduce an interface from the deletion. The functional impact of Δexon3 on intact RyR2 channels remains to be tested.

Flexible Cysteine Pairs

RyRs have been found to report on oxidative stress, and it has been shown that cysteines play a crucial role in this process (Durham et al., 2008; Eu et al., 2000; Eu et al., 1999; Xu et al., 1998). Each RyR2 monomer contains up to 90 cysteine residues, and seven of these are contained within the NTD. The higher resolution (1.7 Å) of the RyR2 V186M mutant allows us to check into these residues in more detail. Four individual cysteines are arranged in two pairs that display a high degree of flexibility.

 All rights reserved

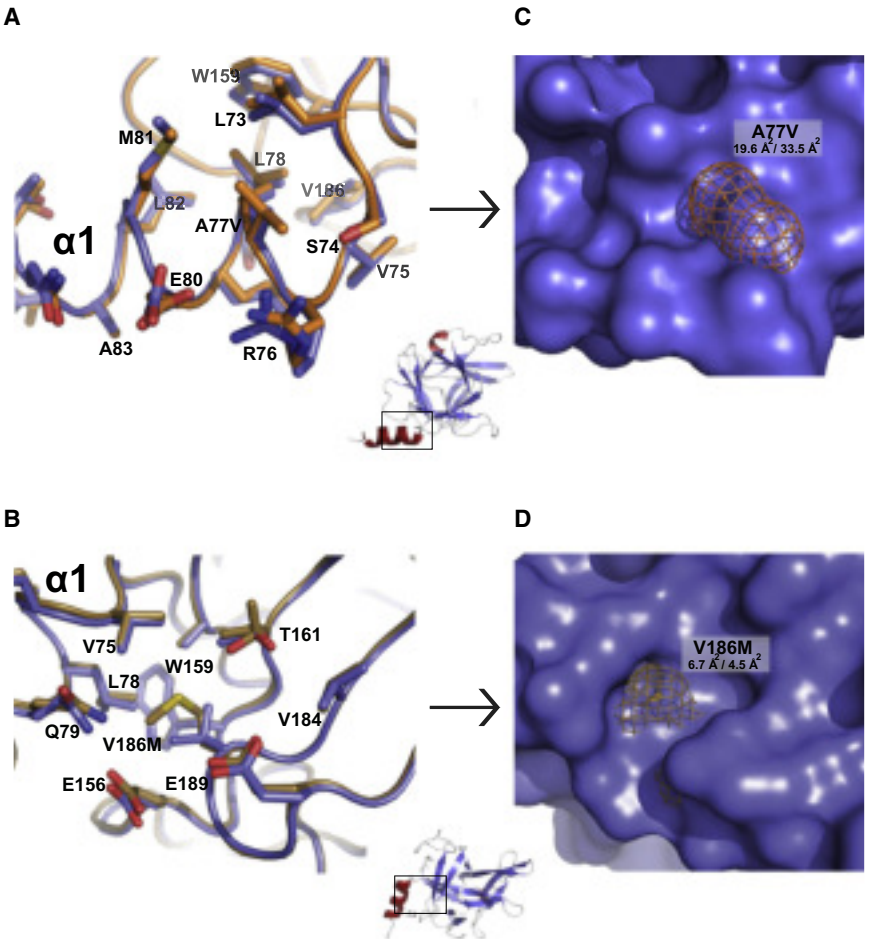

Figure 3. RyR2 A77V and V186M Mutations Cause Distinct Changes in the Surface

(A) Superposition of RyR2 wild-type (blue) and RyR2 A77V (orange) in the region surrounding the mutation. Nitrogen atoms are shown as dark blue, oxygen in red, and sulfur in yellow. The inset shows the view (box) relative to the full domain.

(B) Superposition of RyR2 wild-type (blue) with RyR2 V186M (brown).

(C and D) Surface representation of RyR2 wild-type (blue) with the surface of the superposed A77V and V186M mutations shown as a mesh. The views are identical to the ones for the corresponding Figures 3A and 3B. The A77V and V186M mutations alter the local surface. Numbers shown are solvent accessible areas, with the first number for the wild-type residue, and the second for the mutant.

The first pair, consisting of C36 and C65, is located on β2 and on the loop preceding β4 (Figure 5A). Three distinct conformations are visible for C36, including a position that points to the solvent and a position pointing toward C65. Both residues are conserved among RyR1–3, and mutations of the C36 counterpart in RyR1 have been implicated in MH (Lynch et al., 1997). A similar arrangement exists for C131 (on β6) and C158 (on the β7-β8 loop): in this case, both adopt dual conformations pointing either toward or away from one another (Figure 5B). C158 is partially exposed to solvent in one conformation. This second cysteine pair is not conserved, because C131 is present only in RyR2. Neither of the cysteines was modeled as cystine bonds in the V186M structure.

The hypothesis therefore arises whether any of these cysteines could report on redox state by formation of a disulfide bond or by receiving a modification. Indeed, it has been shown that RyR1 counterpart C36 can both be S-glutathionylated and oxidized to a disulfide in RyR1 (Aracena-Parks et al., 2006). Whether the C131/C158 pair can undergo similar reactions in intact RyR2 remains to be shown.

Comparison with IP3 Receptors

The β trefoil domain is structurally homologous to two domains in the NTD of IP3 receptors (IP3R) (Bosanac et al., 2002; Bosanac et al., 2005), suggesting a strong evolutionary relationship between both Ca^{2+} release channels. By use of the Dali server for finding structural homologs (Holm et al., 2008), the NTD of the IP3 receptor (PDB 1XZZ) (Bosanac et al., 2005) displays the largest structural similarity. The overall fold of the β-trefoil core is conserved, but the structures diverge significantly outside of this core (Figure 6). The single helix in the RyR NTD is replaced by two helices in the IP3R NTD, and both point in a different direction. The RyR loop connecting β1-β2 protrudes further away from the core because of extended β strands, whereas the loop β10-β11 is significantly shortened. In addition, the loops connecting β3-β4, β7-β8, and β8-β9 adopt very different conformations. The different loop conformations, as well as the various amino acid substitutions, drastically alter the overall shape and charge distribution on the surface (Figure S3). This finding suggests that the β-trefoil core serves as a structural template, with distinct functions arising from the various insertions in loops connecting the β strands.

The IP3R contains a second β-trefoil domain (Bosanac et al., 2002), and sequence similarity strongly suggests that such a second β-trefoil domain, immediately downstream in the sequence, is present in RyRs as well (Bosanac et al., 2005; Serysheva et al., 2005, 2008).

DISCUSSION

RyRs play a crucial role in E-C coupling of both skeletal and cardiac muscles: they allow the regulated release of Ca^{2+} from the sarcoplasmic reticulum into the cytoplasm. Their importance is highlighted by the severe impact of sometimes subtle point mutations in their genes. In the skeletal muscle RyR1, these can lead to MH and CCD (Robinson et al., 2006), whereas mutations in the cardiac RyR2 may result in CPVT and ARVD2 (George et al., 2007; Thomas et al., 2007). The RyRs are the largest ion channels currently known (~2.2 MDa), but the amount of atomic

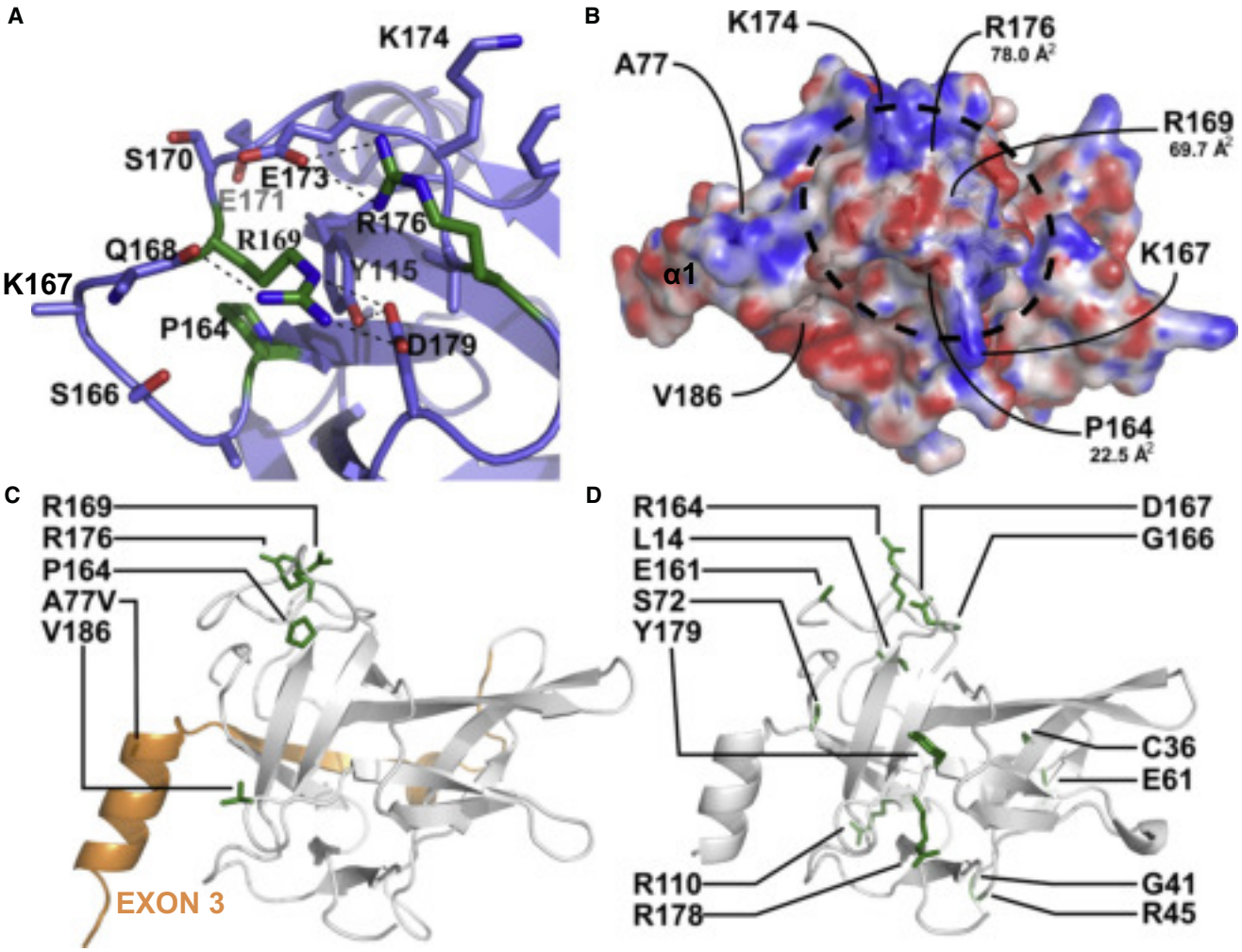

Figure 4. Other Disease Mutations in RyR1 and RyR2

(A) Detail of the RyR2 β8-β9 loop, showing ionic pairs and hydrogen bonds. The view is from the top of Figure 1A, looking down on the loop and the α helix N terminus. Three residues known to cause CPVT or ARVD2 are shown in green. The loop contains two other positively charged residues, K167 and K174, which have not been found as the target of disease mutations. The K167 side chain density was not visible.

(B) Electrostatic potential of the RyR2 NTD, showing that the β8-β9 loop is positively charged. The view is from the top in Figure 1A. Missing side chains were added to allow a more reliable surface potential calculation. The five known disease positions of the RyR2 NTD are indicated for reference, as well as two other positively charged residues in the β8-β9 loop. The circle represents the β8-β9 loop. Numbers shown indicate the solvent accessible surface area for the side chains of P164, R169, and R176.

(C and D) Comparison of the disease positions in RyR2 (left) and RyR1 (right) (rabbit RyR1 numbering), highlighted in green. Disease positions are more spread out in the RyR1 NTD. The portion deleted by the RyR2 Δexon3 mutant is highlighted in orange. The views correspond to the front view of Figure 1A.

resolution data is very limited. This has obstructed detailed insights into RyR function and malfunction.

In this article, we describe the crystal structures of amino terminal domains of RyR1 and RyR2. The proteins fold as a β-trefoil domain with an α-helical segment lining one side. The core of the fold is similar to that found in the NTD of IP3Rs, but significant differences outside the core change the overall shape and charge distribution. We also determined the structures of two RyR2 disease mutants (A77V and V186M) known to cause CPVT and map other known mutations on the surface of both RyR1 and RyR2.

A serious form of CPVT is caused by the removal of a 35 amino acid stretch (exon3) in RyR2 that maps in the NTD (Bhuiyan et al., 2007; Marjamaa et al., 2009). The more drastic phenotype associated with this deletion correlates with the expected large impact on the structure. In contrast, none of the point mutations investigated so far seems to affect either the overall structure or the stability of the domain, but instead alters a local environment. This leaves the only possibility that these local surfaces are involved in binding other RyR domains or auxiliary proteins. We propose the existence of at least two important interaction sites on the RyR NTD: one involving the loop connecting β8 and β9 and another involving the α helix with a neighboring pocket.

Three attractive candidates can be proposed to interact with these sites. The first includes the second mutational hot spot

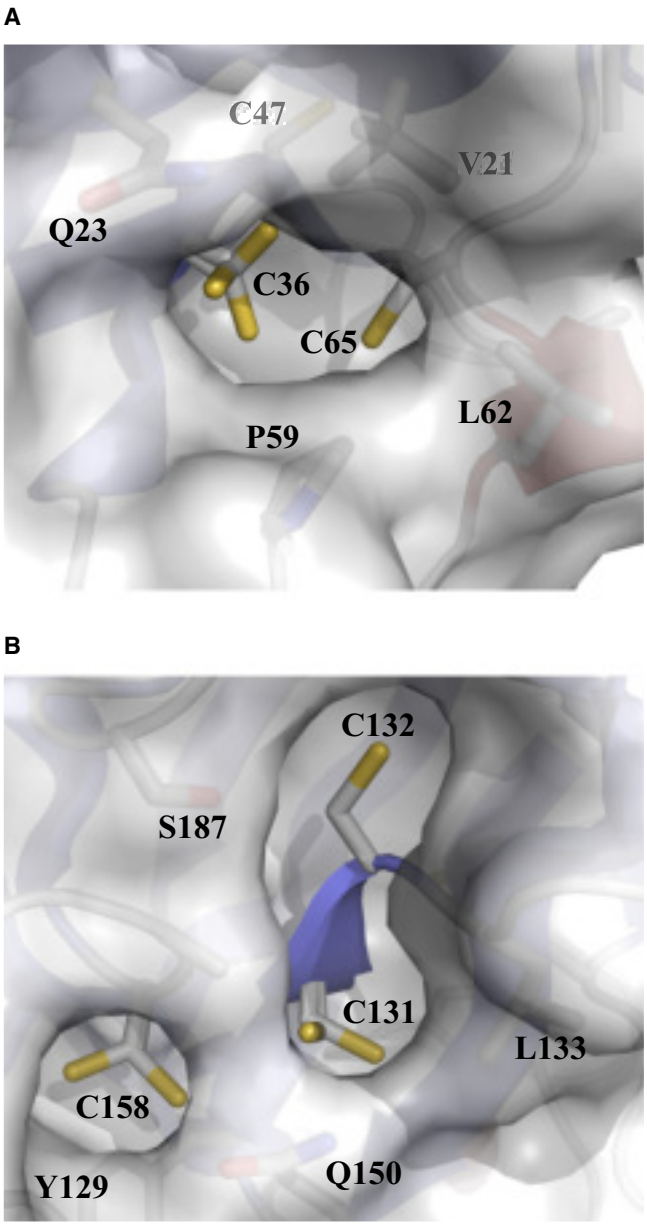

Figure 5. Two Flexible Cysteine Pairs
(A and B) Cysteines with multiple conformations in the RyR2 V186M structure. The surface contributed by the cysteines is taken away for clarity, showing that some cysteines point to the solvent in distinct conformations. Select residues are labeled for orientation. C36 is shown in 3 different conformations, whereas both C131 and C158 have dual conformations. C65 and C132 only displayed single conformations.

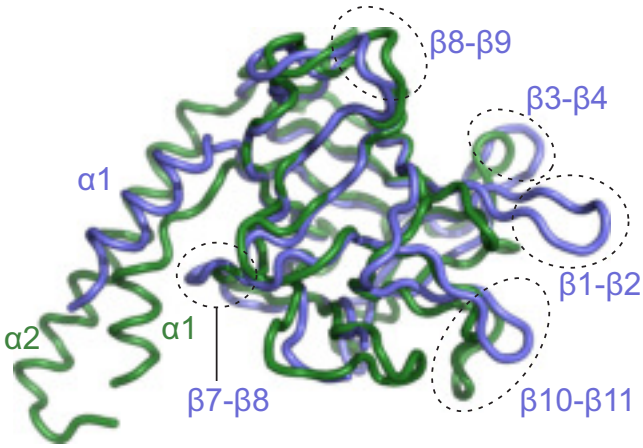

Figure 6. Comparison with the IP3 Receptor NTD
Superposition of the RyR2 NTD (blue) with the IP3R NTD (green). Loops with the most significant differences are highlighted (RyR2 labeling). The view corresponds to the front view in Figure 1A.

of RyR1 and RyR2. The so-called "zipper hypothesis" suggests an interaction between the N-terminal and central hot spot regions, and mutations in either region can cause destabilization of a domain-domain interaction that is required for normal channel function (Ikemoto and Yamamoto, 2002). A second candidate is FKBP12. This hypothesis comes from a combination of modeling and docking studies, suggesting that the NTD is located in the clamp region (Serysheva et al., 2008). In this model, a number of mutations, including mutations in the β8-β9 loop of the NTD, are also surface exposed in the entire RyR1 structure. Because FKBP12 has been shown to map to the same region (Samso et al., 2006; Wagenknecht et al., 1997), the mutations could directly interfere with its binding. However, deletion of the first 305 residues in RyR2 does not abolish FKBP12.6 binding (Masumiya et al., 2003), so the contribution of these sites to FKBP12.6 binding can only be minor. A third possibility is an interaction between the NTD and the domains immediately downstream in the sequence. In IP3Rs, the NTD is known to affect the binding affinity of IP3 to a cleft formed by the two downstream domains, suggesting a direct domain-domain interaction (Bosanac et al., 2005). RyR1–3 residues ~220–600 display sequence similarity with the corresponding region in IP3Rs, and it is therefore possible that a similar domain-domain interaction is conserved.

Although the mutations in the RyR2 NTD seem to cluster in two distinct spots, a number of mutations in the RyR1 NTD are more scattered across the surface. Although it is possible that RyR2 mutations in other regions of the NTD may be found in the future, one possibility is that Ca^{2+} handling in cardiac myocytes is more crucial for survival than in skeletal muscle and that the corresponding mutations in RyR2 would be fatal. Whether the scattered mutations in RyR1 influence the domain stability or have no long-range effects on the structure remains to be determined.

With the availability of a 9.6 Å cryoEM structure of an entire RyR1 channel (Ludtke et al., 2005), the natural question arises about the location of the NTD in the overall protein. We have performed extensive docking experiments with our NTDs using the program SITUS (Wriggers et al., 1999). The docking results vary greatly depending on the exact method used (Figure S5). With Laplacian filtering, the crystal structure docks in the so-called subregion 4a, a position close the central cavity of the RyR (Figure S5). However, elegant experiments involving the addition of GST or GFP to N-terminal regions of RyR2 and RyR3 have shown difference density in a region near the clamp (Liu et al., 2001; Wang et al., 2007). These fusion proteins still retained wild-type channel properties, suggesting that the overall impact

on the folding was minimal. Because the N terminus of the docked domain points to the central cavity, the overall length of GST (~33 Å between N terminus and C terminus) is insufficient to support difference density at >90 Å away. Other solutions are incompatible for the same reason (Figure S5).

Docking without Laplacian filtering places models in subregion 5. Although this is close to a previously proposed site (Serysheva et al., 2005, 2008), even here caution is required, because all of the top 5 solutions have very similar correlation values. These solutions dock to the same site but with completely different orientations, resulting in ~90° relative rotations. Deducing the precise location of individual amino acids within the full-length RyR is therefore premature.

Because reliable docking into a cryoEM map depends greatly on the relative size, it is possible that the size of the NTD (~4% of one RyR monomer) is simply too small to allow reliable docking at this resolution. We conclude that either more experimental restraints or higher resolution cryoEM maps are necessary to allow a precise location and orientation of the RyR NTD.

The crystal structure of the NTD is only one step closer toward a complete high-resolution understanding of RyR structure and function. Besides an overall description of the protein fold, our results highlight two distinct interaction interfaces that are required for normal RyR function. More high-resolution structures will be necessary to increase our understanding of the largest ion channel currently known.

It should be noted that, during preparation of this manuscript, coordinates for a RyR1 NTD crystal structure were deposited in the PDB database by F. Amador and co-workers (PDB ID 3HSM), and the results were recently published (Amador et al., 2009). Their structure is very similar to our independently solved RyR1 NTD structure. However, no structures of the RyR2 NTD or any disease mutants had been reported by this group. One finding of these authors was that the β8-β9 loop forms a mutational "hot spot," which corresponds to one of our two proposed interaction sites.

EXPERIMENTAL PROCEDURES

Cloning, Expression, and Purification

Rabbit RyR1 (residues 9–205), mouse RyR2 (residues 1–217), and human RyR3 (residues 10–207) were cloned into a modified pET28 vector containing, in tandem, a His-tag, MBP, and a TEV cleavage site, followed by the construct of interest (Van Petegem et al., 2004). Mutations were made using the Quikchange protocol (Stratagene). Proteins were expressed at 30°C or 37°C in *E. coli* Rosetta (DE3) pLacI strains (Novagen), induced at OD_{600} of ~0.6 with 0.2 mM IPTG, and were grown for 4 more hours prior to harvesting. Cells were lysed via sonication in buffer A (250 mM KCl and 10 mM HEPES [pH 7.4]) with 25 μg/ml DNaseI and 25 μg/ml lysozyme, were applied to a PorosMC column (Tosoh Biosep), were washed with 5 column volumes (CV) of buffer A and 5 CV of buffer A plus 10 mM imidazole, and were eluted with buffer B (250 mM KCl plus 500 mM imidazole [pH 7.4]). The protein was dialyzed overnight against buffer A and was cleaved simultaneously with recombinant TEV protease. The samples were then run on another PorosMC column in buffer A, and the flowthrough was collected and dialyzed against buffer C (10 mM KCl plus 20 mM Tris-Cl [pH 8.8]), applied to a ResourceQ column (GE Healthcare), and eluted with a gradient from 0% to 40% buffer D (1 M KCl plus 20 mM Tris-Cl [pH 8.8]). Finally, the samples were run on a Superdex200 (GE Healthcare) gel filtration column in buffer A. The protein samples were exchanged to 10 mM KCl plus 5 mM HEPES (pH 7.4), concentrated to 10–20 mg/ml using Amicon concentrators (10K MWCO; Millipore), and stored at −80°C.

Crystallization and Data Collection

All crystals were obtained by hanging drop vapor diffusion. Wild-type RyR2 NTD crystals appeared in 0.5–1.5M malonate (pH 4.0). The best crystals for RyR2 A77V and V186M were obtained in 0.1 M malonate (pH 4.6–4.9) plus 5%–20% saturated $(NH_4)_2SO_4$. RyR1 NTD crystals appeared in 0.1 M Bis-Tris (pH 7.0) plus 15%–25% PEG3350. Crystals were transferred to paratone oil and flash-frozen in liquid N_2 prior to data collection. The datasets were collected at the Stanford Synchrotron Radiation Lightsource (SSRL) beamline 11-1 and the Canadian Light Source (CLS) beamline 08ID-1, and were processed using the HKL2000 package (HKL Research). Data collection statistics are available in Table 1.

Structure Solution and Refinement

A molecular replacement search model was designed, consisting of a minimal β-trefoil domain (IP3R NTD, PDB ID 1XZZ), stripped from all loops and with all side chains truncated to alanine. Molecular replacement was performed with Phaser (McCoy et al., 2007). Because of the poor initial phasing power of the search model, we used the data set with the highest diffraction (1.7 Å for RyR2 V186M) and obtained an initial model via autobuilding procedures implemented in ARP/wARP (Langer et al., 2008). The model was completed by successive rounds of manual model building in COOT (Emsley and Cowtan, 2004) and refinement with REFMAC5.5 (Murshudov et al., 1997). A simulated annealing composite omit map was calculated with CNS (Brunger et al., 1998) to verify the absence of residual model bias (Figure S1A). The RyR2 WT and A77V structures were solved by using the refined V186M structure as a molecular replacement model. For RyR1, the molecular replacement model consisted of the RyR2 NTD structure with all nonidentical amino acids truncated to alanine. Side chains with missing densities were not modeled but were included in the electrostatic calculations with APBS (Baker et al., 2001). The number of molecules in the asymmetric unit are two (RyR2 WT), one (A77V and V186M), and nine (RyR1). One chain in the RyR1 structure has poor electron density and was only modeled partially (chain I).

The final refinement statistics can be seen in Table 1. The slightly elevated R and Rfree factors are most likely due to the presence of a long loop (residues 88–109) for which there was significant difference density but that could not be modeled (Figure S1B). The exception is W98, which we modeled inside a hydrophobic pocket for the following reasons: the corresponding density shows up for both wild-type chains and both point mutants in weighted difference maps and a composite map; its location in the middle of the flexible loop places it at the expected position; the density is especially clear for the 1.7 Å V186M data, with the distinct features of a tryptophan side chain containing a hole in the aromatic ring (Figure S1C); its location in a hydrophobic pocket is a preferred chemical location; and the electron density at this site does not show up for any of the 9 RyR1 chains that do not have a tryptophan in this loop. All structure figures were prepared using PYMOL (DeLano Scientific, San Carlos).

Thermal Melting Curves

The protein melting curves were measured by means of thermofluor experiments (Nettleship et al., 2008). Samples for melting curves contained 50 μl of 0.2 mg/ml protein and 1× SYPRO Orange solution (Invitrogen) using manufacturer's instructions. The melts were obtained in a DNA engine opticon 2 real-time PCR machine (BIORAD), using the SYBR green filter option. The temperature was changed from 20°C to 95°C in 0.5°C steps. At every step, the temperature was kept constant for 15 s. The melting temperatures were obtained by taking the maxima of the first derivative of the melting curve (RyR2 Δexon3) or by taking the midpoint of each transition (all other samples).

ACCESSION NUMBERS

Coordinates of the structures have been deposited in the RCSB database with PDB accession codes 3IM5, 3IM6, 3IM7, and 3ILA.

SUPPLEMENTAL DATA

Supplemental data include five figures and can be found with this article online at http://www.cell.com/structure/supplemental/S0969-2126(09)00373-6.

ACKNOWLEDGMENTS

We thank the staff and beamline scientists at the Canadian Light Source (Saskatoon, Canada) and the Stanford Synchrotron Radiation Laboratory (Palo Alto, CA) for providing access to their beamlines and providing technical support; Wayne Chen (University of Calgary) for the full-length RyR2 clone and useful comments on our manuscript; Kurt Beam (University of Colorado) for the RyR1 clone; and Eric Jan (University of British Columbia) for use of the real-time PCR instrument. F.V.P. is a CIHR new investigator and a MSFHR career investigator. This work is funded by a grant from the Heart and Stroke Foundation of British Columbia and Yukon Territories and by the Canadian Foundation for Innovation and the BC Knowledge Development Fund. P.L solved the RyR1 NTD structure and measured the melting curves. F.V.P. designed the experiments and solved the structures of the wild-type and mutant RyR2 NTDs. The authors declare no conflict of interest.

Received: June 22, 2009
Revised: August 12, 2009
Accepted: August 22, 2009
Published: November 10, 2009

REFERENCES

Amador, F.J., Liu, S., Ishiyama, N., Plevin, M.J., Wilson, A., MacLennan, D.H., and Ikura, M. (2009). Crystal structure of type I ryanodine receptor amino-terminal beta-trefoil domain reveals a disease-associated mutation "hot spot" loop. Proc. Natl. Acad. Sci. USA *106*, 11040–11044.

Aracena-Parks, P., Goonasekera, S.A., Gilman, C.P., Dirksen, R.T., Hidalgo, C., and Hamilton, S.L. (2006). Identification of cysteines involved in S-nitrosylation, S-glutathionylation, and oxidation to disulfides in ryanodine receptor type 1. J. Biol. Chem. *281*, 40354–40368.

Baker, N.A., Sept, D., Joseph, S., Holst, M.J., and McCammon, J.A. (2001). Electrostatics of nanosystems: application to microtubules and the ribosome. Proc. Natl. Acad. Sci. USA *98*, 10037–10041.

Bers, D.M. (2004). Macromolecular complexes regulating cardiac ryanodine receptor function. J. Mol. Cell. Cardiol. *37*, 417–429.

Bhuiyan, Z.A., van den Berg, M.P., van Tintelen, J.P., Bink-Boelkens, M.T., Wiesfeld, A.C., Alders, M., Postma, A.V., van Langen, I., Mannens, M.M., and Wilde, A.A. (2007). Expanding spectrum of human RYR2-related disease: new electrocardiographic, structural, and genetic features. Circulation *116*, 1569–1576.

Bosanac, I., Alattia, J.R., Mal, T.K., Chan, J., Talarico, S., Tong, F.K., Tong, K.I., Yoshikawa, F., Furuichi, T., Iwai, M., et al. (2002). Structure of the inositol 1,4,5-trisphosphate receptor binding core in complex with its ligand. Nature *420*, 696–700.

Bosanac, I., Yamazaki, H., Matsu-Ura, T., Michikawa, T., Mikoshiba, K., and Ikura, M. (2005). Crystal structure of the ligand binding suppressor domain of type 1 inositol 1,4,5-trisphosphate receptor. Mol. Cell *17*, 193–203.

Brunger, A.T., Adams, P.D., Clore, G.M., DeLano, W.L., Gros, P., Grosse-Kunstleve, R.W., Jiang, J.S., Kuszewski, J., Nilges, M., Pannu, N.S., et al. (1998). Crystallography & NMR system: A new software suite for macromolecular structure determination. Acta Crystallogr. D Biol. Crystallogr. *54*, 905–921.

Durham, W.J., Aracena-Parks, P., Long, C., Rossi, A.E., Goonasekera, S.A., Boncompagni, S., Galvan, D.L., Gilman, C.P., Baker, M.R., Shirokova, N., et al. (2008). RyR1 S-nitrosylation underlies environmental heat stroke and sudden death in Y522S RyR1 knockin mice. Cell *133*, 53–65.

Emsley, P., and Cowtan, K. (2004). Coot: model-building tools for molecular graphics. Acta Crystallogr. D Biol. Crystallogr. *60*, 2126–2132.

Eu, J.P., Xu, L., Stamler, J.S., and Meissner, G. (1999). Regulation of ryanodine receptors by reactive nitrogen species. Biochem. Pharmacol. *57*, 1079–1084.

Eu, J.P., Sun, J., Xu, L., Stamler, J.S., and Meissner, G. (2000). The skeletal muscle calcium release channel: coupled O2 sensor and NO signaling functions. Cell *102*, 499–509.

George, C.H., Jundi, H., Thomas, N.L., Fry, D.L., and Lai, F.A. (2007). Ryanodine receptors and ventricular arrhythmias: emerging trends in mutations, mechanisms and therapies. J. Mol. Cell. Cardiol. *42*, 34–50.

Giannini, G., Conti, A., Mammarella, S., Scrobogna, M., and Sorrentino, V. (1995). The ryanodine receptor/calcium channel genes are widely and differentially expressed in murine brain and peripheral tissues. J. Cell Biol. *128*, 893–904.

Holm, L., Kaariainen, S., Rosenstrom, P., and Schenkel, A. (2008). Searching protein structure databases with DaliLite v.3. Bioinformatics *24*, 2780–2781.

Ikemoto, N., and Yamamoto, T. (2002). Regulation of calcium release by interdomain interaction within ryanodine receptors. Front. Biosci. *7*, d671–d683.

Langer, G., Cohen, S.X., Lamzin, V.S., and Perrakis, A. (2008). Automated macromolecular model building for X-ray crystallography using ARP/wARP version 7. Nat. Protoc. *3*, 1171–1179.

Liu, Z., Zhang, J., Sharma, M.R., Li, P., Chen, S.R., and Wagenknecht, T. (2001). Three-dimensional reconstruction of the recombinant type 3 ryanodine receptor and localization of its amino terminus. Proc. Natl. Acad. Sci. USA *98*, 6104–6109.

Ludtke, S.J., Serysheva, I.I., Hamilton, S.L., and Chiu, W. (2005). The pore structure of the closed RyR1 channel. Structure *13*, 1203–1211.

Lynch, P.J., Krivosic-Horber, R., Reyford, H., Monnier, N., Quane, K., Adnet, P., Haudecoeur, G., Krivosic, I., McCarthy, T., and Lunardi, J. (1997). Identification of heterozygous and homozygous individuals with the novel RYR1 mutation Cys35Arg in a large kindred. Anesthesiology *86*, 620–626.

Marjamaa, A., Laitinen-Forsblom, P., Lahtinen, A.M., Viitasalo, M., Toivonen, L., Kontula, K., and Swan, H. (2009). Search for cardiac calcium cycling gene mutations in familial ventricular arrhythmias resembling catecholaminergic polymorphic ventricular tachycardia. BMC Med. Genet. *10*, 12.

Masumiya, H., Wang, R., Zhang, J., Xiao, B., and Chen, S.R. (2003). Localization of the 12.6-kDa FK506-binding protein (FKBP12.6) binding site to the NH2-terminal domain of the cardiac Ca^{2+} release channel (ryanodine receptor). J. Biol. Chem. *278*, 3786–3792.

Maximciuc, A.A., Putkey, J.A., Shamoo, Y., and Mackenzie, K.R. (2006). Complex of calmodulin with a ryanodine receptor target reveals a novel, flexible binding mode. Structure *14*, 1547–1556.

McCoy, A.J., Grosse-Kunstleve, R.W., Adams, P.D., Winn, M.D., Storoni, L.C., and Read, R.J. (2007). Phaser crystallographic software. J. Appl. Crystallogr. *40*, 658–674.

Murshudov, G.N., Vagin, A.A., and Dodson, E.J. (1997). Refinement of macromolecular structures by the maximum-likelihood method. Acta Crystallogr. D Biol. Crystallogr. *53*, 240–255.

Nettleship, J.E., Brown, J., Groves, M.R., and Geerlof, A. (2008). Methods for protein characterization by mass spectrometry, thermal shift (ThermoFluor) assay, and multiangle or static light scattering. Methods Mol. Biol. *426*, 299–318.

Robinson, R., Carpenter, D., Shaw, M.A., Halsall, J., and Hopkins, P. (2006). Mutations in RYR1 in malignant hyperthermia and central core disease. Hum. Mutat. *27*, 977–989.

Rueffert, H., Olthoff, D., Deutrich, C., Meinecke, C.D., and Froster, U.G. (2002). Mutation screening in the ryanodine receptor 1 gene (RYR1) in patients susceptible to malignant hyperthermia who show definite IVCT results: identification of three novel mutations. Acta Anaesthesiol. Scand. *46*, 692–698.

Samso, M., Shen, X., and Allen, P.D. (2006). Structural characterization of the RyR1-FKBP12 interaction. J. Mol. Biol. *356*, 917–927.

Samso, M., Wagenknecht, T., and Allen, P.D. (2005). Internal structure and visualization of transmembrane domains of the RyR1 calcium release channel by cryo-EM. Nat. Struct. Mol. Biol. *12*, 539–544.

Serysheva, I.I., Hamilton, S.L., Chiu, W., and Ludtke, S.J. (2005). Structure of Ca^{2+} release channel at 14 A resolution. J. Mol. Biol. *345*, 427–431.

Serysheva, I.I., Ludtke, S.J., Baker, M.L., Cong, Y., Topf, M., Eramian, D., Sali, A., Hamilton, S.L., and Chiu, W. (2008). Subnanometer-resolution electron cryomicroscopy-based domain models for the cytoplasmic region of skeletal muscle RyR channel. Proc. Natl. Acad. Sci. USA *105*, 9610–9615.

Sharma, M.R., Penczek, P., Grassucci, R., Xin, H.B., Fleischer, S., and Wagenknecht, T. (1998). Cryoelectron microscopy and image analysis of the cardiac ryanodine receptor. J. Biol. Chem. *273*, 18429–18434.

Shepherd, S., Ellis, F., Halsall, J., Hopkins, P., and Robinson, R. (2004). RYR1 mutations in UK central core disease patients: more than just the C-terminal transmembrane region of the RYR1 gene. J. Med. Genet. *41*, e33.

Thomas, N.L., George, C.H., Williams, A.J., and Lai, F.A. (2007). Ryanodine receptor mutations in arrhythmias: advances in understanding the mechanisms of channel dysfunction. Biochem. Soc. Trans. *35*, 946–951.

Van Petegem, F., Clark, K.A., Chatelain, F.C., and Minor, D.L., Jr. (2004). Structure of a complex between a voltage-gated calcium channel beta-subunit and an alpha-subunit domain. Nature *429*, 671–675.

Wagenknecht, T., Radermacher, M., Grassucci, R., Berkowitz, J., Xin, H.B., and Fleischer, S. (1997). Locations of calmodulin and FK506-binding protein on the three-dimensional architecture of the skeletal muscle ryanodine receptor. J. Biol. Chem. *272*, 32463–32471.

Wang, R., Chen, W., Cai, S., Zhang, J., Bolstad, J., Wagenknecht, T., Liu, Z., and Chen, S.R. (2007). Localization of an NH(2)-terminal disease-causing mutation hot spot to the "clamp" region in the three-dimensional structure of the cardiac ryanodine receptor. J. Biol. Chem. *282*, 17785–17793.

Wriggers, W., Milligan, R.A., and McCammon, J.A. (1999). Situs: A package for docking crystal structures into low-resolution maps from electron microscopy. J. Struct. Biol. *125*, 185–195.

Wright, N.T., Prosser, B.L., Varney, K.M., Zimmer, D.B., Schneider, M.F., and Weber, D.J. (2008). S100A1 and calmodulin compete for the same binding site on ryanodine receptor. J. Biol. Chem. *283*, 26676–26683.

Xu, L., Eu, J.P., Meissner, G., and Stamler, J.S. (1998). Activation of the cardiac calcium release channel (ryanodine receptor) by poly-S-nitrosylation. Science *279*, 234–237.

Yano, M. (2008). Ryanodine receptor as a new therapeutic target of heart failure and lethal arrhythmia. Circ. J. *72*, 509–514.

Zalk, R., Lehnart, S.E., and Marks, A.R. (2007). Modulation of the ryanodine receptor and intracellular calcium. Annu. Rev. Biochem. *76*, 367–385.

 ©2009 Elsevier Ltd All rights reserved